UC Berkeley
Working Papers

Title
Optimization Tools For Automated Vehicle Systems

Permalink
https://escholarship.org/uc/item/7qn422nz

Author
Shiller, Zvi

Publication Date
1995

eScholarship.org Powered by the California Digital Library
University of California

This paper has been mechanically scanned. Some errors may have been inadvertently introduced.

CALIFORNIA PATH PROGRAM
INSTITUTE OF TRANSPORTATION STUDIES
UNIVERSITY OF CALIFORNIA, BERKELEY

Optimization Tools for Automated Vehicle Systems

Zvi Shiller

University of California, Los Angeles

California PATH Working Paper
UCB-ITS-PWP-95-10

This work was performed as part of the California PATH Program of the University of California, in cooperation with the State of California Business, Transportation, and Housing Agency, Department of Transportation; and the United States Department Transportation, Federal Highway Administration.

The contents of this report reflect the views of the authors who are responsible for the facts and the accuracy of the data presented herein. The contents do not necessarily reflect the official views or policies of the State of California. This report does not constitute a standard, specification, or regulation.

July 1995

ISSN 1055-1417

Optimization Tools for Automated Vehicle Systems

Zvi Shiller
Department of Mechanical, Aerospace and Nuclear Engineering
University of California, Los Angeles
Los Angeles, CA 90095
shiller@seas.ucla.edu

Abstract

This work addresses the issue of emergency maneuvers, treated in the context of time-optimal control. The vehicle is modeled as a planar rear-drive, front steering, vehicle, with three degrees-of-freedom in the plane, and two control inputs: the steering angle and the rear tractive force. The tire side forces are approximated by a piecewise linear saturation function, and are coupled to the longitudinal force by the friction ellipse, derived from the Dugoff model. To compute the time optimal trajectories, we first solve the inverse dynamics problem, i.e. compute the nominal (open loop) control inputs that would drive the vehicle along a specified path at given speeds. The vehicle's orientation along the given path is determined by numerically integrating the moment equation from known initial conditions. The two control inputs are then computed using the remaining equations of motion. Parameterizing the path by its arc length, we transform the equations of motion to functions of the vehicle's speed and acceleration along the path. We then derive constraints on the vehicle's speeds and accelerations due to the saturation of the tire forces and path geometry. The performance limit along a specified maneuver is then computed by minimizing the motion time along the path, assuming free initial and final speeds. This establishes the velocity limit curve, which serves as an upper bound for any feasible trajectory. The fastest trajectory is therefore the one that slides along the velocity limit curve. This optimization scheme is demonstrated numerically for a lane change maneuver.

Kewords: vehicle dynamics, optimal control, emergency maneuvers, safety.

Executive Summary

This report summarizes the work accomplished during the first year of the project "Optimization tools for Intelligent Vehicles", MOU 125. The focus of this work is on computing time-optimal maneuvers, which might be used to develop strategies for emergency maneuvers and to establish the vehicle's performance envelope.

In this work, we address the problem of emergency maneuvers in the context of time optimal control. Specifically, we compute time optimal trajectories along specified paths for a nonlinear vehicle model, which considers both lateral and longitudinal motions. Minimizing motion time is a suitable frame work for computing emergency maneuvers because, in addition to minimizing the disturbance to the traffic flow, time optimal trajectories represent the ultimate vehicle's performance between given boundary conditions, which might be needed in true emergency conditions.

To compute time optimal trajectories, we first solve the inverse dynamics problem, i.e., compute the nominal (open loop) control inputs required to traverse a specified trajectory. We consider ground vehicles with front steering and a rear-drive (and brake), modeled in the plane with three degrees-of-freedom, using the steering angle and the rear tractive force as the two control variables. The vehicle is assumed to move at given speeds along a specified path. The vehicle's orientation is determined by integrating the moment equation. The steering angle and the tractive force along the specified path are computed from the two force equations. The kinematic solution for the body slip angle, assuming zero speeds and no tire slip, is also developed to help predict vehicle behavior at low speeds.

The vehicle's performance limits are determined in the form of limiting trajectories by solving an optimal control problem that minimizes the motion time with free initial and final speeds. The optimization problem is solved as a parameter optimization, using exact penalty functions to account for the control constraints. The optimal trajectories, which are shown to slide along the control and the geometric path constraints, represent the upper bounds on vehicle's speeds. They can be used for planning emergency maneuvers, and for verifying that a given trajectory is dynamically feasible, and hence dynamically safe. Examples of high speed lane change maneuvers are presented.

1 Introduction

This report summarizes the work accomplished during the first year of the project "Optimization tools for Intelligent Vehicles", MOU 125. The focus of this work is on computing time-optimal maneuvers, which might be used to develop strategies for emergency maneuvers and to establish the vehicle's performance envelope.

Vehicle control has been traditionally studied for separate longitudinal or lateral motions. Extensive studies have been conducted on the longitudinal control problem, which concerns the control of the longitudinal speed or displacement using the engine torque as the control input (Peng and Tomizuka 1990,Sheikholeslam and Desoer 1992,Godbole and Lygeros 1994). Other studies have focused on lateral control, which concerns the control of the yaw motion, assuming a constant longitudinal speed, using the steering angle and the engine torque as the control inputs (Peng and Tomizuka 1991,Hessburg and Tomizuka 1991,Hessburg et. al. 1991,Chee and Tomizuka 1994). Fewer studies have addressed the combined longitudinal and lateral motion problem (Narendran and Hedrick 1993).

In (Peng and Tomizuka 1991,Hessburg and Tomizuka 1991,Hessburg et. al. 1991), optimal preview control and a fuzzy logic controller were developed for lane following, based on a linearized vehicle model, and considering lateral motions only. In (Chee and Tomizuka 1994), these controllers were modified for lane change maneuvers, and were tested in simulations for a lane change at 110 km/h. While this speed might be considered extreme, the lane transition was rather long, lasting $6s$ over $180m$[1]. In (Narendran and Hedrick 1993), a sliding mode controller was developed for lane change maneuvers, considering a combined lateral and longitudinal vehicle model, and tested in numerical simulations at nominal conditions.

Though satisfactory for moderate conditions, controllers based on linear models were found ineffective for emergency maneuvers, at which simultaneous steering and braking are required at high lateral accelerations (Smith and Starkey 1994). In that study, a controller for emergency maneuvers was developed by optimizing the gains of a linear controller over the step response of the nonlinear model. The resulting controller was tested successfully in simulations at $30m/s$ (about 70 MPH) over a $60m$ lane transition. However, the controller gains are path and speed specific, which hinders the applicability of this method for general emergency maneuvers. Clearly, the emergency maneuvering problem is far from solved, and a better understanding of the vehicle's performance at high speeds is needed before effective controllers for emergency conditions can be developed.

In this work, we address the problem of emergency maneuvers in the context of time optimal control. Specifically, we compute time optimal trajectories along specified paths for a nonlinear vehicle model, which considers both lateral and longitudinal motions. Minimizing motion time is a suitable frame work for computing emergency maneuvers because, in addition to minimizing the disturbance to the traffic flow,

[1] In our present work, the vehicle traverses a lane change transition of $60m$ in less than 2s

time optimal trajectories represent the ultimate vehicle's performance between given boundary conditions, which might be needed in true emergency conditions.

To compute time optimal trajectories, it is necessary to first solve the inverse dynamics problem, i.e., compute the nominal (open loop) control inputs required to traverse a specified trajectory. For this task, we consider ground vehicles with front steering and a rear-drive (and brake), modeled in the plane with three degrees-of-freedom, using the steering angle and the rear tractive force as the two control variables. The vehicle is assumed to move at given speeds along a specified path. Since this specifies only the positions of the mass center, or two of the vehicle's three degrees-of-freedom in the plane, the vehicle's orientation remains to be determined.

Writing the equations of motion in the body frame, it is shown that the vehicle's orientation is constrained by the moment equation, which is a second order differential equation in the body slip angle (the angle between the body axis and the velocity of its mass center). Numerically integrating this equation yields the vehicle's orientation, which depends on path geometry and on vehicle parameters and speeds. The steering angle and the tractive force along the specified path are computed from the two force equations, once the body slip angle along the path has been computed. The kinematic solution for the body slip angle, assuming zero speeds and no tire slip, is also developed, requiring the numerical integration of a first order differential equation. It can be used to predict vehicle behavior at low speeds.

The vehicle's performance limits are determined in the form of limiting trajectories by solving an optimal control problem that minimizes the motion time with free initial and final speeds. The optimization problem is solved as a parameter optimization, using exact penalty functions to account for the control constraints. This essentially maps the control constraints to the trajectory space. The optimal trajectories, which are shown to slide along the control and the geometric path constraints, represent the upper bounds on vehicle's speeds. They can be used for planning emergency maneuvers, and for verifying that a given trajectory is dynamically feasible, and hence dynamically safe. This approach to computing the performance limits is more constructive than previous work, which establishes the performance limits by simulating vehicle dynamics along various maneuvers, then observing the control inputs that result in spin or skid (Allen et. al. 1991).

This work was summarized in (Shiller and Sundar 1995). The optimization routines, enhanced with computer graphics, were implemented in FORTRAN and C on a Silicon Graphics workstation.

This report describes the main tasks for the first year:

1. Develop vehicle model
2. Select an appropriate tire model
3. Formulate velocity and acceleration limits
4. Optimize motion time along specified paths.

2 Vehicle Model

In selecting the vehicle model, we evaluated the complex model developed by Lunger and adopted by Tomizuka (Peng and Tomizuka 1990). Because of the large number of states used in this model, we decided to consider first the two dimensional bicycle model. It ignores the load shift due to roll and pitch, but it accounts for the side forces of the front and rear wheels, which are nonlinear functions of the front and rear slip angles, respectively. To practically solve the inverse dynamics problem, we approximated the tire forces by a piecewise linear saturation function of the slip angle. The two control inputs are assumed to be the front steering angle and the rear tractive/braking force. The front wheel is assumed to provide only a side force, and no tractive force or resistance. This model has only six independent states: the position of the mass center in the plane, vehicle's orientation, and their time derivatives. The complex model will be later used in dynamic simulations for evaluating the nominal controls computed for the simplified model.

We first derive the kinematic relations between the slip angles of the front and rear wheels and the steering angle of the planar bicycle model shown in figure 1, with front steering and rear driving (and braking). The inertial coordinate frame is denoted by XY, and the body fixed frame, centered at the mass center, is denoted by xy. The angle of the vehicle's x axis in the inertial frame is φ; the angle of the linear velocity of its mass center, in the body frame, is α; and the steering angle of the front wheel in the body frame is β. All angles are positive in the counter clockwise direction.

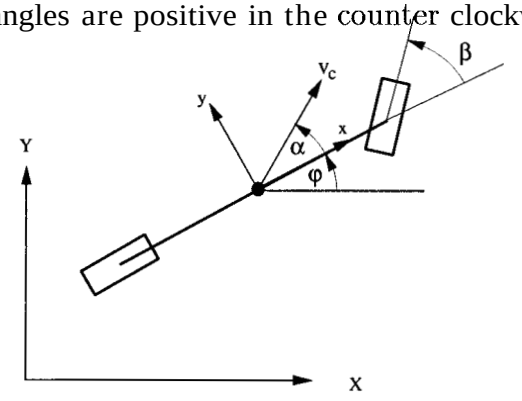

Figure 1: The bicycle model

Figure 2 shows the vehicle at a typical point along a specified path. The velocity of the mass center coincides with the path tangent and is at an angle θ relative to the inertial frame. Thus,

$$\varphi = \theta - \alpha \tag{1}$$

For general motions, the vehicle undergoes pure rotation around some instantaneous center, located at p (the instantaneous radius) from the mass center, as shown in figure 2. Note that $p > 0$ for a counterclockwise turn, and $p < 0$ for a clockwise turn.

The linear velocity of every point on the vehicle is perpendicular to the line from that point to the instantaneous center. The angles between the linear velocities of the

rear and front wheels and their major axes are the rear and front slip angles, a, and α_f, shown in figure 2. Consistent with this notation, we call α the body *slip angle.*

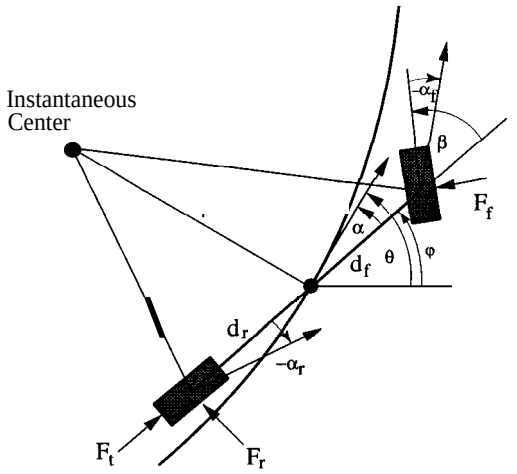

Figure 2: The slip angles

The wheel slip angles can be derived as explicit functions of α and the instantaneous curvature:

$$\mathbf{CY} = tan-'[\frac{-d_r\kappa + \sin\alpha}{\cos \mathrm{CY}}] \tag{2}$$

$$\alpha_f = r - P \tag{3}$$

where

$$\gamma = tun^{-1}[\frac{d_f\kappa + \sin\alpha}{\cos \mathrm{CY}}], \tag{4}$$

$d,$ and d_f are the distances between the mass center and the centers of the rear and front wheels, respectively, and $\kappa = 1/\rho$ is the instantaneous curvature. Henceforth, we will denote p and κ as the instantaneous radius and curvature, and R and K as the radius and curvature corresponding to the specified path. An equivalent representation of the slip angles, in terms of the Cartesian coordinates, is

$$\alpha_r = tun-'[\frac{-d_r\dot{\varphi} + \mathrm{y}\cos\varphi - \dot{x}\sin\varphi}{x\cos\varphi + \dot{y}\sin\varphi}] \tag{5}$$

$$\alpha_f = tan-'[\frac{d_f\dot{\varphi} + \dot{y}\cos\varphi - \dot{x}\sin\varphi}{\dot{x}\cos\varphi + \dot{y}\sin\varphi}] - \beta \tag{6}$$

where x and $\dot{y}$ represent the velocity of the mass center in the inertial frame.

For transient motions, the instantaneous center does not necessarily coincide with the center of path curvature. This can be seen by recognizing that the instantaneous center of the rotating body satisfies

$$\frac{1}{\rho} = \kappa = \frac{\dot{\varphi}}{\dot{s}} = \varphi_s = \theta_s - \alpha_s \tag{7}$$

where the subscript s denotes derivatives with respect to $s \in [0, s_f]$, the path arc length. Similarly, the center of path curvature satisfies

$$\frac{1}{R} = K = \theta_s \tag{8}$$

Hence, path curvature coincides with the curvature of the rotating body if and only if $a, = 0$, i.e. $\alpha =$ constant. The two are identical for steady-state motions since then the slip angle, a, is constant.

The external forces acting on the vehicle consist of the tire forces shown in figure 2. The front tire generates only a side force, F_f, since the front wheel is assumed to rotate freely. The rear tire generates both side, F_r, and longitudinal, F_t, forces due to the engine torque or brakes. Treating F_t as a control input, we ignore motor and drive train dynamics. The actual engine input can later be computed for the resulting tractive force, using the inverse dynamics of the tire and drive train subsystem.

To simplify the computation of the control inputs, we derive the equations of motion in the body frame, and express the moment equation around the center of the front wheel:

$$F_t - F_f \sin(\beta) = ma, \tag{9}$$

$$F_r + F_f \cos(\beta) = ma, \tag{10}$$

$$-(d_f + d_r)F_r = I\ddot{\varphi} - md_f a_y \tag{11}$$

where m is the vehicle mass, and a, and a_y are the projections of the absolute acceleration of the mass center on the body frame.

This formulation partially decouples the equations of motion in terms of the controls: the moment equation is not explicit in the controls; the force equation in the x direction includes only F_t, and the remaining force equation includes both F_t and β. This formulation also makes clear that the angular acceleration, $\ddot{\varphi}$, cannot be arbitrarily specified, since F_r is a state dependent force. The moment equation (11) is, therefore, an equality constraint that eliminates one of the vehicle's three degrees-of-freedom. It will be used to compute the vehicle's orientation along a specified path.

3 Tire model

We have studied several tire models, including those developed by Dugoff (1970) and Sakai (1981). The Dugoff model is an empirical model, providing analytical relations for the longitudinal and lateral forces as functions of the slip angle and slip ratio. It thus accounts for the coupling between the side and longitudinal forces, known as the *friction ellipse.*

The Dugoff model for a typical tire is (Dugoff 1970)[2]

$$F_x = -\frac{C_s s}{1-s} f(\lambda) \tag{12}$$

$$F_y = -\frac{C_\alpha \tan\alpha}{1-s} f(\lambda) \tag{13}$$

where

$$\lambda = \frac{\mu W(1-\epsilon v\sqrt{s^2+\tan^2\alpha})(1-s)}{2\sqrt{c_s^2 s^2 + C_\alpha^2 \tan^2\alpha}} \tag{14}$$

$$f(\lambda) = \begin{cases} \lambda(2-\lambda) & \text{for } \lambda < 1 \\ 1 & \text{for } \lambda > 1 \end{cases} \tag{15}$$

and

F_x = longitudinal force
F_y = side force
s = longitudinal slip
a = tire slip angle
C_s = cornering stiffness
C_α = longitudinal stiffens
W = vertical load
v = vehicle speed
μ = coefficient of road adhesion
ϵ = adhesion reduction coefficient

Figure 3 shows the longitudinal and side forces for various slip angles at fixed tire parameters. These curves can be approximated by ellipses, with major axes dependent on the slip angle:

$$\left(\frac{F_x}{F_{xmax}(\alpha)}\right)^2 + \left(\frac{F_y}{F_{ymax}(\alpha)}\right)^2 = 1 \tag{16}$$

$F_{ymax}(\alpha)$ is computed by setting the slip ratio $s = 0$ in (13), whereas $F_{xmax}(\alpha)$ is approximated by:

$$F_{xmax}(\alpha) = \lim_{s\to 1} F_x(\alpha) = \frac{C_s W \mu(1-\epsilon v\sqrt{1+\tan^2\alpha})}{\sqrt{c_s^2 + C_\alpha^2 \tan^2\alpha}} \tag{17}$$

The Sakai model is theoretical, based on modeling of the tire/road interaction (Sakai 1981). The longitudinal and side forces computed by this model are coupled

[2]In this section, we use α to denote the *tire* slip angle

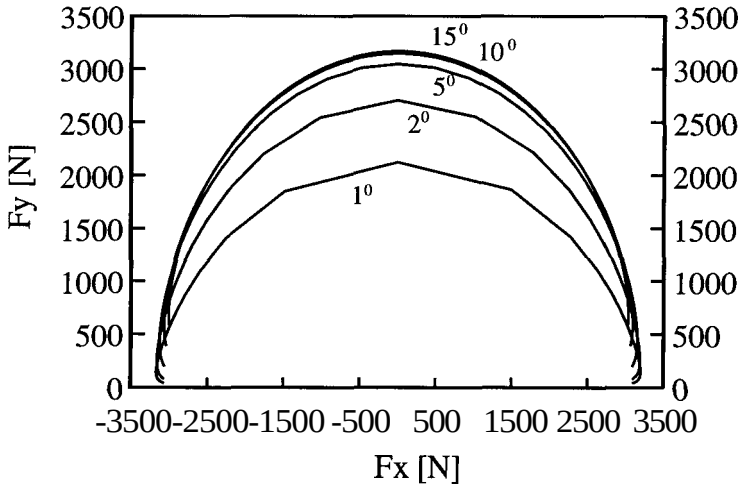

Figure **3:** The Dugoff model.

by elliptical curves which better approximate the experimental data than the Dugoff model. However, the Dugoff model is simpler, and its friction ellipse easy to compute (Maalej et. al. 1989). In addition, the Dugoff model underestimates the actual tire forces, which might be beneficial for computing safe emergency maneuvers.

Using either tire model would severely couple the equations of motion with the tractive force, making the inverse dynamics problem difficult to solve. For simplicity, we, therefore, ignore the friction ellipse at low slip angles, representing the tire side forces by the piecewise linear saturation function

$$F_r = \begin{cases} -C_\alpha \alpha & \text{if } |\alpha| < \alpha^* \\ -C_\alpha \alpha^* & \text{if } a \geq \alpha^* \\ C_\alpha \alpha^* & \text{if } \alpha \leq -\alpha^* \end{cases} \tag{18}$$

where α^* is the critical tire slip angle, corresponding to the maximum side force. The tractive force, F_t, is generated by the forward slip of the rear wheel, independent of the slip angle. However, we do limit the vector sum of the tractive and the side forces to be within a friction ellipse that is fixed at the critical slip angle

$$(\frac{F_t}{A(\alpha^*)})^2 + (\frac{F_r}{B(\alpha^*)})^2 \leq 1 \tag{19}$$

where $A(\alpha^*)$ and $B(\alpha^*)$ are constants?corresponding to the major axes of the friction ellipse at $\alpha = \alpha^*$. Here, the vertical load, W, is constant due to the assumption of a planar bicycle model. In future work, we will modify W as a function of the forward acceleration to account for the longitudinal load shift.

4 Inverse Dynamics

To solve the inverse dynamics problem, we substitute the tire model (18) (only the first linear segment) into the equations of motion, to yield

$$F_t + C_f \alpha_f \sin(@) = m a, \tag{20}$$

$$F_r - C_f \alpha_f \cos(\beta) = m a_y \tag{21}$$

$$(d_f + d_r) C_r \alpha_r = I \ddot{\varphi} - m d_f a_y \tag{22}$$

where C_r and C_f are the coefficients of the cornering stiffness of the rear and front tires, respectively. Since both, F_f and F_r, are functions of the body slip angle, a , it is necessary to first determine the vehicle's orientation for given path and speeds, using (22). We can then compute β, using (21), and F_t, using (20). The vehicle's path and speeds are defined by the time histories of the location, $\mathbf{x}(t)$, of the mass center.

The computation of a is first presented for kinematic conditions, assuming zero slip. For curved motions, this is equivalent to assuming zero speeds, since it is only at zero speeds that the vehicle can follow a curved path with zero lateral tire forces.

4.1 Kinematic α

The assumption of zero slip implies that the velocities of the rear and front wheels coincide with their major axes, or $\alpha_r = \alpha_f = 0$, as shown in figure 4. It follows that at every point along the path

$$\rho \sin(\alpha) = d, \tag{23}$$

Using (7) we obtain a first order differential equation in a:

$$\alpha_s(s) + \frac{1}{d_r} \sin(\alpha(s)) = \theta_s(s) \tag{24}$$

Note that the forcing function of (24) is path curvature, $\theta_s(s)$.

We can solve for the kinematic a, α_k, by numerically integrating (24), starting at known initial conditions. We can then solve for the corresponding steering angle, β_k, using the trigonometric relation (see figure 4):

$$tan(\beta_k) = \frac{d_r + d_f}{d_r} tan(\alpha_k) \tag{25}$$

The kinematic solution for a and β might be used as close approximations of the transient solution at low speeds.

Note that any α other than α_k would result in a nonzero rear slip angle, a_r. Assuming a counter clockwise turn, we obtain that $a < \alpha_k \rightarrow a_r < 0$, and $a > \alpha_k \rightarrow a_r > 0$. Therefore, the vehicle will spin if $a < \alpha_k$ along a counter clockwise turn, since then the direction of the rear force is opposite of the instantaneous center.

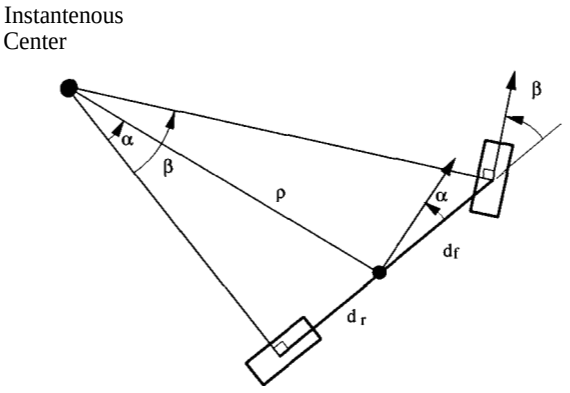

Figure 4: Kinematic motion

4.2 Dynamic α

To compute the dynamic (transient) a, we first represent the velocity and acceleration of the mass center in terms of the speed and acceleration along the path. This is done by parameterizing the path by the path arc length, s E $[0, s_f]$, so that any point along the specified path is represented by the vector function $\mathbf{x}(s) = \{x(s), y(s)\}$. Differentiating **x** once with respect to s yields the unit tangent **x,;** differentiating twice yields the normal **x,,** of magnitude $|| \mathbf{x}_{,,} || = K$, where $|| \ . \ ||$ denotes the Euclidean norm. The velocity, v,, and acceleration, **a,,** of the center of mass, can be expressed in terms of the speed, $\dot{s}$, and acceleration, $\ddot{s}$, tangent to the path:

$$\mathbf{v}_c = \dot{s}\mathbf{x}_s \tag{26}$$

$$\mathbf{a}_{,} = \ddot{s}\mathbf{x}_s + \dot{s}^2\mathbf{x}_{ss} \tag{27}$$

It is easy to show that the components of the absolute acceleration (27) in the body frame, are:

$$a, = \ddot{s}\cos(\alpha) - \dot{s}^2 K \sin(\alpha) \tag{28}$$

$$a_y = \mathrm{s}\sin(\alpha) + \dot{s}^2 K \cos(a) \tag{29}$$

The angular velocity and acceleration can also be expressed in terms of the speed and tangent acceleration:

$$\theta - \dot{\alpha} = (\theta_s - \alpha_s)\dot{s} \tag{30}$$

$$\ell - a = (\theta_s - \alpha_s)\ddot{s} + (\theta_{ss} - \alpha_{ss})\dot{s}^2 \tag{31}$$

We can now write (22) as a second order differential equation in a:

$$(d_r + d_f)C_r\alpha_r = I[(\theta_s - \alpha_s)\ddot{s} + (\theta_{ss} - \alpha_{ss})\dot{s}^2] - md_f[\ddot{s}\sin(\alpha) + \dot{s}^2\theta_s\cos(\alpha)] \tag{32}$$

where

$$\alpha_r = tan^{-1}[\frac{-d_r(\theta_s - \alpha_s) + \sin(\alpha)}{\cos(a)}1] \tag{33}$$

Solving for α_{ss} yields

$$\alpha_{ss} = -(d_f + d_r)\alpha_r(\alpha)\frac{C_r}{I\dot{s}^2} - \frac{m}{I}d_f\frac{\ddot{s}}{\dot{s}^2}\sin(\alpha) - a_s\frac{s}{\dot{s}^2} + (\frac{s}{\dot{s}^2} - \frac{m}{I}d_f\cos(\alpha))\theta_s + \theta_{ss} \quad (34)$$

We can compute $\alpha(s)$ by numerically integrating α_{ss} from known initial conditions, using θ_s and θ_{ss} as the forcing functions. It is convenient to integrate from steady-state motion along straight line segment, for which $\alpha(s) = \alpha_s(s) = 0$.

Note that θ_{ss} is defined only for continuous path curvatures. At points where the curvature is discontinues, a, is also discontinuous. To compute the discontinuity in α_s, we integrate $\theta_{ss} - a,,$ with respect to s across the discontinuity

$$\int_{s_-}^{s_+}(\theta_{ss} - \alpha_{ss})ds = (\theta_s(s) - \alpha_s(s))]_{s_-}^{s_+} = \varphi_s]_{s_-}^{s_+} = \frac{\dot{\varphi}}{\dot{s}}]_{s_-}^{s_+} = 0 \quad (35)$$

This integral equals zero since $\dot{\varphi}$ and $\dot{s}$ are continuous everywhere. Therefore,

$$\alpha_s(s_+) = \alpha_s(s_-) + \Delta\theta_s(s) \quad (36)$$

The jump in a, is, thus, equal to the jump in θ_s.

Figure 6 shows the dynamic a for motions at various constant speeds along the path shown in figure 5. This path consists of a B-spline, which is C^2 continuous. As a result, a is smooth and differentiable for all speeds. The kinematic a, shown in figure 6 as a dotted line, was computed using (24).

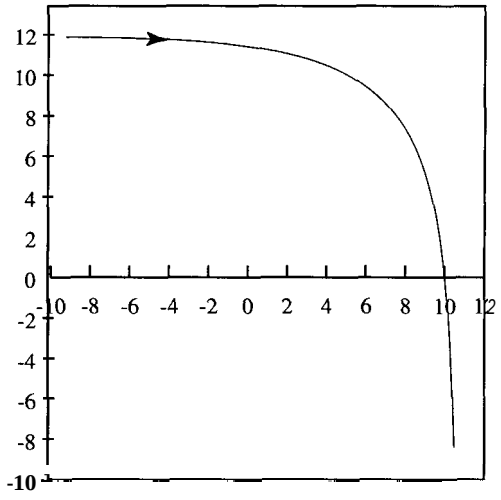

Figure 5: A B spline path

Figure 8 shows the dynamic a for the path shown in figure 7, consisting of two straight line segments, connected by a circular arc. Clearly, the curvature along this path is discontinuous across the junctions between the straight lines and the circular

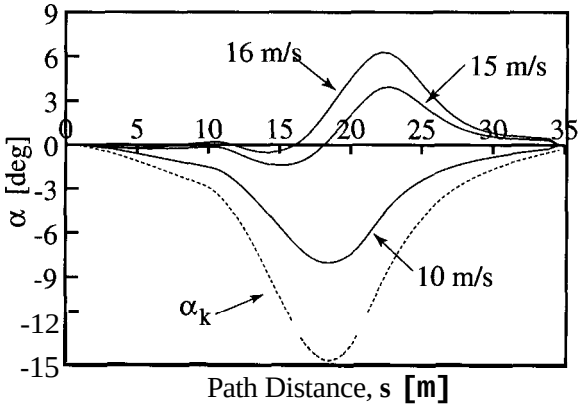

Figure 6: Dynamic α for various speeds along the B spline path

arc. At these points, α_s (the slope of α) is also discontinuous, as can be seen in figure 8. Here, α exhibits a typical response of an under-damped second order system as it oscillates, following each step in the curvature. These oscillations depend on the vehicle speed, as can be explained by substituting into **(34)** $\ddot{s} = 0$, assuming small α and α_r, and considering a straight line path ($\theta_s = \theta_{ss} = 0$), to yield:

$$\alpha_{ss} + \frac{C_r d_r (d_f + d_r)}{I\dot{s}^2}\alpha_s + \frac{C_r (d_f + d_r)}{I\dot{s}^2}\alpha = 0 \tag{37}$$

Clearly, **(37)** represents a second order system in α with a damping ratio, ζ, inversely proportional to $\dot{s}$:

$$\zeta = \sqrt{\frac{C_r d_r^2 (d_f + d_r)}{4I\dot{s}^2}} \tag{38}$$

Therefore, α would oscillate as a result of a nonzero forcing function or nonzero initial conditions. The higher the speed, the larger the oscillations, as we have observed. Also, the damping ratio is proportional to d_r, the distance of the mass center from the rear axle. Therefore, the closer the center of mass to the front axle, the more damped the oscillations.

4.3 Steady-State α

To gain insights into the behavior of the dynamic α, we investigate steady-state motions along a circular arc, along which α and θ_s are constant. With these assumptions, **(32)** reduces to

$$\alpha_r = \frac{-m d_f \dot{s}^2 \theta_s}{(d_r + d_f) C_r} \cos(\alpha) \tag{39}$$

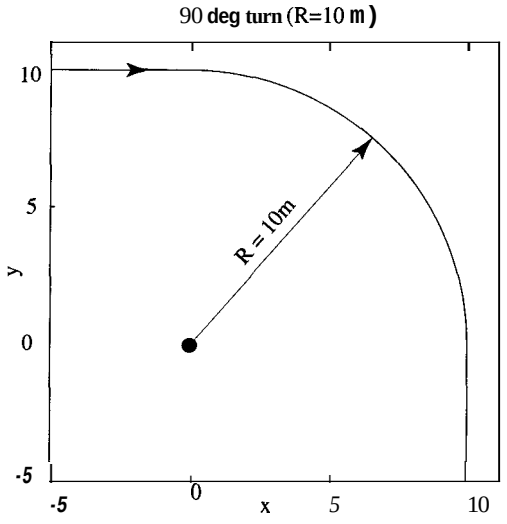

Figure 7: **A** Circular turn

where

$$a, = tan^{-1}[\frac{-d_r\theta_s + \sin(\alpha)}{\cos(a)}] \qquad (40)$$

To solve for the steady-state a, we intersect (39) and (40), as shown schematically in figure 9 for two values of $\dot{s}$ along a counter clockwise turn **(0,** $= \kappa > 0$). For nonzero $\dot{s}$, (39) is a cosine with an amplitude proportional to $\dot{s}^2$, whereas (40) is close to a straight line, crossing the horizontal axis at α_k. For this turn, as $\dot{s}$ increases, the amplitude of the cosine curve increases, moving the intersection point left of α_k. Therefore, a decreases with speed along the counter clockwise turn, changing from a positive value (the rear wheel inside the curve) at low speeds to a negative value (the rear wheel outside the curve) at high speeds, as shown in figure 10. Also shown in figure 10 is the steady-state β, which is discussed next.

Driving at a negative a, referred to as "drifting a car through a bend", is common in competitive driving of rear-driven cars (Frere 1992). This type of driving is better observed on loose or slippery ground since the amplitude of the cosine in (39) is inversely proportional to the cornering stiffens, C_r. **A** lower stiffens, or a larger amplitude, makes the variations in a with respect to $\dot{s}$ more pronounced.

4.4 Computing β

Once α is known, we can use (10) to solve for the steering angle, β. Rewriting (10) and using (29), yields

$$-C_r\alpha_r - C_f(tan^{-1}[\frac{d_f\kappa + \sin(a)}{\cos(a)}] - \beta)\cos(@) = m(\ddot{s}\sin(\alpha) + \dot{s}^2 K\cos(\alpha)) \qquad (41)$$

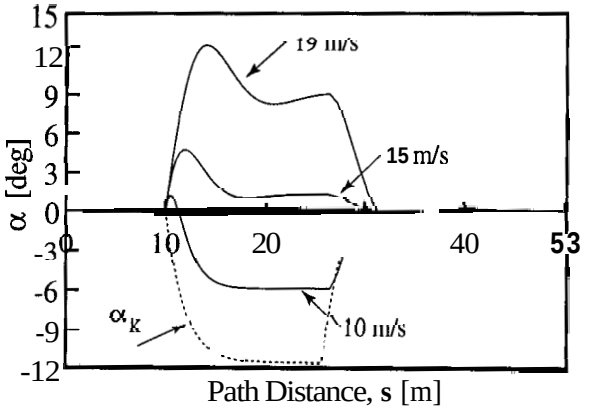

Figure 8: Dynamic a along the circular arc

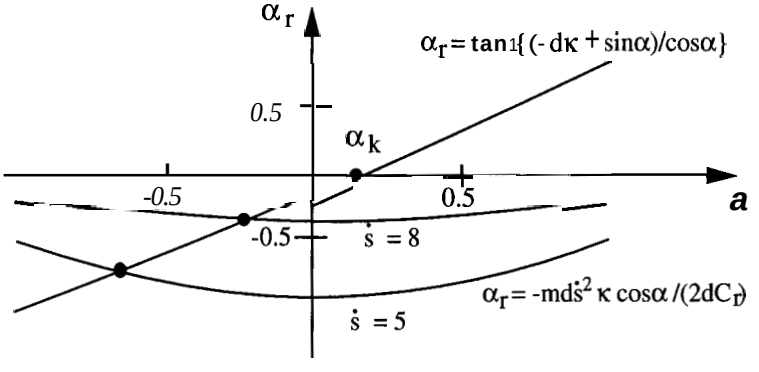

Figure 9: Solving for the steady-state α

To solve for β, we rewrite (41) as

$$(a_1 - \beta)\cos(\beta) = a_2 \tag{42}$$

where

$$a_1 = tan^{-1}[\frac{d_f\kappa + \sin(a)}{\cos(a)}] \tag{43}$$

$$a_2 = -\frac{C_r}{C_f}\alpha_r - \frac{m}{C_f}(\ddot{s}\sin(\alpha) + \dot{s}^2 K\cos(\alpha)) \tag{44}$$

Plotting both sides of (42) reveals two possible solutions in the range $\beta = [-\pi/2, \pi/2]$, as shown in figure 11 for $a_1 = 0.1$. We choose the solution that ensures continuity of β, starting from known initial conditions ($\beta = 0$ along an initial straight line segment). Figure 11 also reveals that a solution for β might not exist for a too high or too low

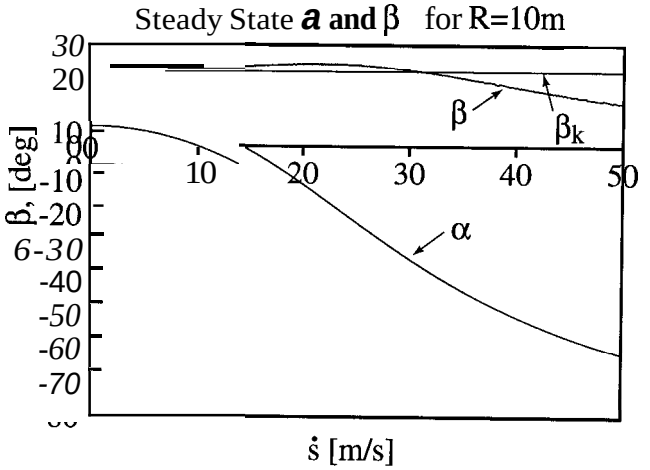

Figure 10: Steady-state a and β along a counter clockwise turn

a_2. The trajectory must, therefore, satisfy at all $s \in [0, s_f]$ two constraints of the form

$$a_2 - a_{2max} \leq 0 \tag{45}$$

$$-a_2 + a_{2min} \leq 0 \tag{46}$$

where

$$a_{2max} = \max_{\beta \in [-\beta_{max}, \beta_{max}]} (a_1 - \beta)\cos(\beta) \tag{47}$$

$$a_{2min} = \min_{\beta \in [-\beta_{max}, \beta_{max}]} (a_1 - \beta)\cos(\beta) \tag{48}$$

in order to be dynamically feasible, and β_{max} represents the physical limit on the steering angle due to the steering mechanism:

$$|\beta| \leq \beta_{max}. \tag{49}$$

A trajectory segment might be infeasible if the acceleration component parallel to the y body axis, a_y, is too high, either because of a too high acceleration, speed, or path curvature.

This solution for β is valid only if the resulting $|\alpha_f| < \alpha_f^*$. Otherwise, we set the front lateral tire force, F_f, in (10) to its maximum value

$$F_f = F_f^* = -C_f \alpha_f^* sign(\alpha_f) \tag{50}$$

and solve for β, using:

$$\cos\beta = \frac{-1}{C_f \alpha_f^* sign(\alpha_f)} [F_r(\alpha) + m(\ddot{s}\sin a + \dot{s}^2 K \cos\alpha)] \tag{51}$$

Fwhere γ was defined in (4), and $sign(\cdot)$ is the signum function. Obviously, the right hand side of (51) should be in the interval $[-1,1]$ for a solution to exist. This in turn imposes a constraint on $\dot{s}$ and $\ddot{s}$, as discussed later. Alternatively, we can constrain β so that $|\alpha_f|$ does not exceed α_f^*.

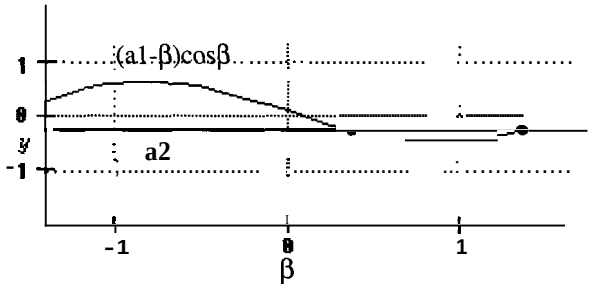

Figure 11: Typical curve of $y = (x - a)\cos(x)$ with $a = 0.1$.

Figure 10 shows the steady-state steering angle at various speeds along a counter clockwise turn of $10m$ radius. For this vehicle, the steering angle stays close to its kinematic value, $\beta_k = 22.1^o$, until about $31m/s$, then it drops gradually to about 12" at $50m/s$. It is interesting to note that the constraints (45) and (46) were not active for the steady-state solution at any speed, whereas these constraints were active at relatively low speeds for the transient solutions. This suggests that the steady-state steering angle is a poor approximation of the actual steering angle during extreme conditions.

Figures 12 and 13 show the steering angles for various constant speeds along the paths shown in figures 5 and 7, respectively. For the B-spline path (figure 12), one of the constraints **(45)** and (46) was violated for speeds exceeding $16m/s$, whereas for the circular turn (figure 13), this occurred above $20m/s$. The other constraint on β, (49), was not imposed in these computations.

Note the discontinuities and oscillations in β in figure 13 due to the discontinuities in path curvature, as compared to the smooth β at all speeds in figure 12. Because of the dynamics of the steering actuator, it would actually be impossible to follow the circular path at all but the lowest speeds. This strongly suggests that sharp transitions between straight and curved road segments are undesirable.

Once β has been computed for the entire path, the tractive force, F_t, is computed from the remaining equation of motion (9), subject to (16).

Experience shows that it is generally difficult to plan a high speed velocity profile along a curved path without violating the steering angle constraint, mainly due to the oscillatory nature of α. It is therefore useful to transform the control constraints to the phase plane, $s - \dot{s}$, to produce upper bounds on vehicle speeds along the path, then plan dynamically feasible, and hence safe, trajectories in that plane, as discussed next.

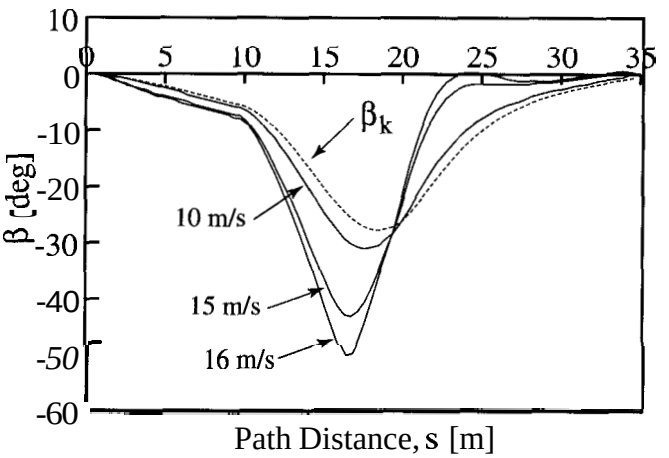

Figure **12:** Dynamic β for various speeds along the B-spline path

5 Velocity and acceleration constraints

In planning emergency maneuvers, it is essential to avoid exceeding the tire force limits to prevent spin or skid. This can be done by mapping the tire force constraints to constraints on the vehicle's speed and acceleration, of the form

$$\ddot{s}_{min} \leq \ddot{s} \leq \ddot{s}_{max} \tag{52}$$

$$\dot{s} \leq \dot{s}_{max} \tag{53}$$

then using these bounds to verify that a given velocity profile along the path is indeed dynamically feasible.

The bounds on the acceleration, $\ddot{s}_{max}$ and $\ddot{s}_{min}$, are computed by, respectively, maximizing or minimizing $\ddot{s}$ over F_t and β, at any given $(s, \dot{s}, \alpha, \alpha_s)$. Considering first the constraints on β, we substitute **(44)** into **(45)** and **(46),** to yield, respectively, for $\alpha > 0$:

$$\ddot{s} \geq \frac{1}{\sin\alpha}[-\dot{s}^2 K \cos\alpha - \frac{1}{m}(C_r\alpha_r + C_f a_{2max})] \tag{54}$$

$$\ddot{s} \leq \frac{1}{\sin\alpha}[-\dot{s}^2 K \cos\alpha - \frac{1}{m}(C_r\alpha_r + C_f a_{2min})] \tag{55}$$

Using the condition that the right hand side of **(51)** is within the interval $[-1, 1]$ yields for $\alpha > 0$

$$\ddot{s} \leq \frac{1}{m\sin\alpha}[F_r(\alpha) - m\dot{s}^2 K \cos\alpha + C_f\alpha_f^*] \tag{56}$$

$$\ddot{s} \geq \frac{1}{m\sin\alpha}[F_r(\alpha) - m\dot{s}^2 K \cos\alpha - C_f\alpha_f^*] \tag{57}$$

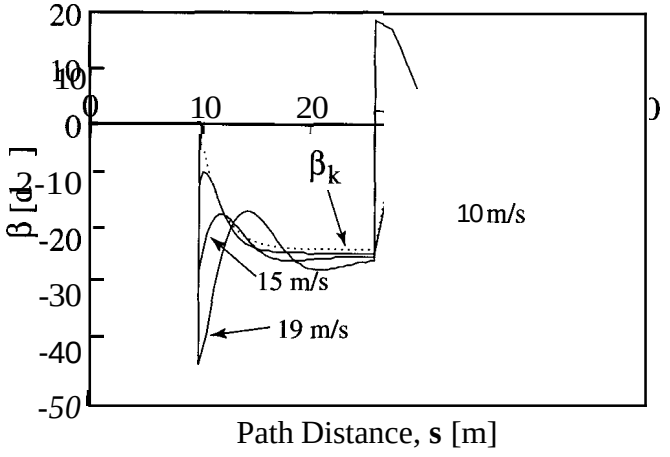

Figure 13: Dynamic β along the circular path

and vice versa for $a < 0$.

Now, assuming constant upper and lower limits on F_t due to the maximum engine torque and the maximum braking force

$$F_{tmin} \leq F_t \leq F_{tmax} \tag{58}$$

we obtain, considering the force equation (9),

$$\ddot{s} \leq \frac{1}{m \cos a}[m\dot{s}^2 K \sin a - F_f(\alpha) \sin \beta + F_{tmax}] \tag{59}$$

$$\ddot{s} \geq \frac{1}{m \cos a}[m\dot{s}^2 K \sin a - F_f(\alpha) \sin \beta + F_{tmin}] \tag{60}$$

Considering the friction ellipse (16), we obtain:

$$\ddot{s} \leq \frac{1}{m \cos \alpha}[A\sqrt{1 - (\frac{F_r}{B})^2} + C_f(\gamma - \beta) \sin \beta + m\dot{s}^2 K \sin \alpha] \tag{61}$$

$$\ddot{s} \geq \frac{1}{m \cos \alpha}[-A\sqrt{1 - (\frac{F_r}{B})^2} + C_f(\gamma - \beta) \sin \beta + m\dot{s}^2 K \sin \alpha] \tag{62}$$

Thus, $\ddot{s}_{max}$ is computed by evaluating (55) and (56), maximizing (59) and (61) over β, and selecting the lower of those values. The lower bound, $\ddot{s}_{min}$ is computed similarly, using (54), (57), (60), and (62), and selecting the higher of those values. It is interesting to note that the bounds on $\ddot{s}$ are nonlinear in β, but linear in the bounds on F_t. Therefore, maximizing or minimizing $\ddot{s}$ is achieved by maximizing or minimizing F_t, respectively, if none of the constraints on β, F_f, and F_r are active.

We assumed that the upper bounds are higher than the lower bounds on S. This might not always be the case, giving rise to constraints on $\dot{s}$. The upper bound on $\dot{s}$ can be determined by computing the lowest value of $\dot{s}$ for which the upper bound on S for any one of the constraints is equal to the lower bound of the same constraint.

The bounds on the speed and acceleration apply locally to every point along the velocity profile. However, these bounds cannot guarantee that a trajectory, starting from a feasible initial state, is indeed feasible along the entire path. It is, therefore, useful to determine the set of initial conditions that yield feasible trajectories. This is done by computing the velocity limit curve, which serves as an upper bound on $\dot{s}$ at any given s, assuming $\alpha(0) = \alpha_s(0) = 0$.

6 Velocity Limit Curve

To compute the velocity limit curve along a specified path, we solve the following optimization problem, formulated in terms of path arc length, s, and its time derivatives. Denoting $\mathbf{x} = \{s, \dot{s}\}$, and $u = \ddot{s}$, we have:

$$\min_{u \in U} J = \int_0^{t_f} 1 dt \tag{63}$$

with free final time, subject to system dynamics

$$\dot{x}_1 = x_2 \tag{64}$$
$$\dot{x}_2 = u \tag{65}$$

subject to control constraints (52)

$$u_{min}(\mathbf{x}, \mathbf{y}) \leq u \leq u_{max}(\mathbf{x}, \mathbf{y}) \tag{66}$$

the boundary conditions

$$s(0) = s_0 \quad , \quad s(t_f) = s_f \tag{67}$$
$$y_1(0) = 0 \tag{68}$$
$$y_2(0) = 0 \tag{69}$$

where y = {cy,$\dot{\alpha}$} are auxiliary variables, satisfying

$$\dot{y}_1 = y_2 \tag{70}$$
$$\dot{y}_2 = \frac{1}{I}(d_r C_r \alpha_r - d_f C_f(\gamma - \beta)\cos\beta) + \theta_s u + \theta_{ss} x_2^2 \tag{71}$$

and

$$\gamma = tan^{-1}[\frac{d_f(\dot{\theta} - y_2) + x_2 \sin(y_1)}{x_2 \cos y_1}]$$
$$\alpha_r = tan^{-1}[\frac{-d_r(\dot{\theta} - y_2) + x_2 \sin(y_1)}{x_2 \cos y_1}]$$

The boundary conditions on **y** assume that the vehicle is tangent to the path at the initial time. Vehicle speeds at the initial and final times, however, are unspecified to ensure that the fastest velocity profile is being selected.

7 Specified path optimization

The optimization of the vehicle's motion along a specified path is identical to the computation of the velocity profile, except that the initial speed is now specified. The optimal velocity profile is expected to stay below the velocity limit curve so as to satisfy the tire force and engine torque constraints.

A practical solution to this optimization problem is to represent the velocity profile along the path by a B-spline, then minimize the motion time, augmented with penalty functions on the control constraints. This transforms the optimization problem (63) to the following parameter optimization:

$$\min_{\mathbf{a}} J = \int_0^{t_f} 1 dt \tag{72}$$

subject to the same constraints as problem (63), where $\mathbf{a} = \{a_1, a_2, .., a,\}$ represents the variable control points of the velocity profile.

It is easy to show that the optimal control of this optimization problem is bang-bang, i.e. s is either maximized or minimized at all times, since the Hamiltonian, H, is affine in the control:

$$H = 1 + \lambda_1 x_2 + \lambda_2 u \tag{73}$$

where λ_1 and λ_2 are the two co-state variables. Following similar arguments as in (Shiller and Lu 1992), it can be shown that since, excluding singular arcs, $\lambda_2 \neq 0$, the Hamiltonian (73) is minimized only by maximizing or minimizing u E $\ddot{s}$. This is similar to the structure of the optimal control of general robotic manipulators (Shiller and Lu 1992), except that here we have no systematic way to compute the switching points.

We developed an optimization routine, enhanced with interactive computer graphics, that computes the time optimal velocity profile along any given path. The path can be generated interactively by moving the control points on the screen, or generated from a data file of the control points. The initial velocity profile is also generated interactively, or from a data file. Once the velocity profile has been selected, the program computes the kinematic and dynamic steering along the path. The vehicle can then be moved interactively along the path for a visual comparison of the kinematic and dynamic solutions. An on-line dynamic simulation is also available for numerically verifying the correctness of the optimal solution. The evaluation of the vehicle's motions along a specified path is relatively fast, requiring only a few seconds. The computation of the velocity limit curve takes about an hour on an old Silicon Graphics 4D-70.

Table 1: Parameters of the planar vehicle

d_f m	d_r m	m Kg	I Kg-m^2	C_r N/rad	C_f N/rad
2	2	1,550	3,100	80,000	80,000

α_f^*	α_r^*	β_{max}	F_{tmax} N	F_{tmin} N	A N	B N
10"	10°	50"	3,000	-6,000	6,000	5,000

8 Example

In this example, we consider the path shown in figure 14, and the vehicle parameters given in table 1. The path consists of a cubic B-spline, represented by 8 control points. The curvature along this path is continuous, as shown in figure 15. The points of highest curvature are at $s = 62m$ and $s = 79m$.

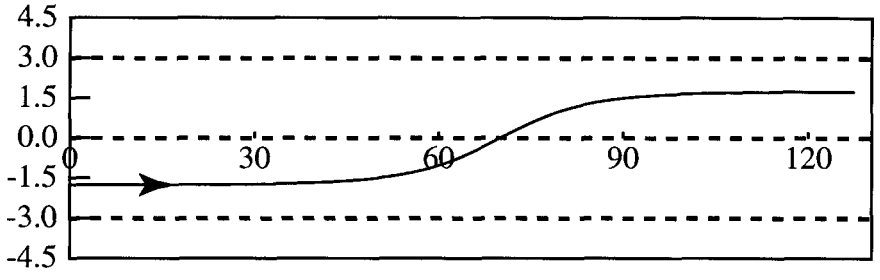

Figure 14: Path for lane change maneuver

First, the velocity limit curve for this maneuver was computed by solving the optimization problem (63), using a parameter optimization. Representing the velocity profile by a B-spline with 11 control points resulted in the velocity limit curve shown in figure 16, and in the corresponding tractive force shown in figure 17. The body slip angle and the steering angle are shown in figures 19 and 20, respectively. The transient steering angle deviates notably from the kinematic steering during the turns.

The velocity limit curve represents the highest speeds at which the vehicle can safely traverse this maneuver, with a motion time of 4.3s. The tangential acceleration, $\ddot{s}$, along the velocity limit curve is shown in figure 18. For the case shown, the vehicle slows down at the maximum deceleration of $3.9m/s^2$. It then switches gradually to the maximum acceleration, which reaches $1.9m/s$. The almost bang-bang structure of the tangential acceleration is expected, as concluded from (73). However, the switch from maximum deceleration to maximum acceleration is gradual due to the continuous representation of the velocity profile, which is C^2 continuous. It is evident from figure 17 that the constraints on the tractive force (58) are dominant along most

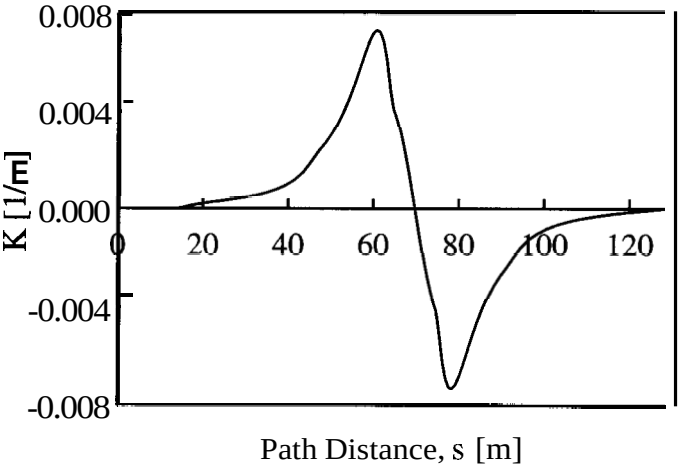

Figure 15: Curvature along the lane change maneuver

of the path, except during the transition between the two peaks in the curvature where (19) is active at the points of highest curvature. No other constraint is active between these points due to the C^2 representation of the velocity profile.

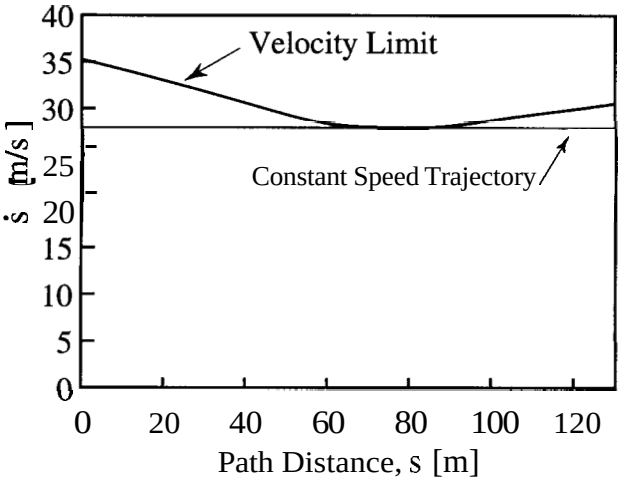

Figure 16: Velocity profiles for the lane change maneuver

Solving (63) with the additional constraint that the vehicle speed remains constant throughout the maneuver, resulted in the maximum constant speed of $27.9m/s$, and a motion time of 4.7s from start to finish. For this case, the maximum constant speed touches the velocity limit curve at its lower point, as shown in figure 16. The active constraint in this case is the friction ellipse (19), which is active at $s = 81m$. The tire slip angles, shown in figure 21, are far from their critical values of 10°, due to the conservative parameters chosen to represent the friction ellipse.

Interestingly, moving at a constant speed along this path does not require braking.

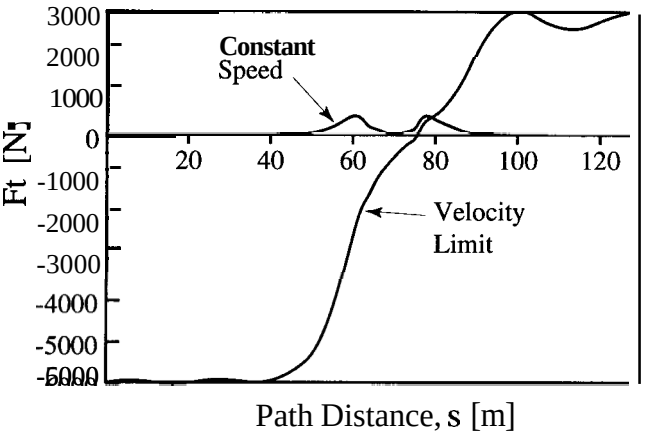

Figure 17: Tractive force for velocity limit and maximum constant speed along lane change maneuver

The tractive force is positive during both left and right turns because the vehicle points inward during each turn, as seen from the slip angle shown in figure 19. Hence, a positive tractive force would have a positive component in the direction of the centripetal acceleration, and thus aid in traversing the turn.

9 Summary

In this project, we have developed a method for generating emergency maneuvers for automated vehicles, considering a planar nonlinear vehicle model with three degrees-of-freedom, and two control inputs: the front steering angle and the rear tractive force. The emergency maneuvers are generated by computing the time optimal velocity profile along a specified path, so as to minimize reaction time, while ensuring that the maneuver is dynamically feasible, and hence safe. To assist in evaluating the dynamic feasibility of a given maneuver, we establish the upper bounds on vehicle performance by solving the time optimal control problem along the specified path with free boundary speeds. This yields the velocity limit curve in the phase plane, $s - \dot{s}$, which serves as an upper bound on *all* feasible velocity profiles. Emergency maneuvers can thus be generated from any initial conditions by selecting a velocity profile that does not cross, but slides along, the velocity limit curve.

Dynamic analysis of the vehicle's performance shows significant deviations between the steady-state and transient motions. It is shown that the steering angle reaches an upper limit, derived from one of the force equations, during transient motions at relatively low speeds, whereas this limit is generally not active during steady-state motions. This suggests that steady-state information is inapplicable for preview control schemes at extreme conditions. The transient steering angle is shown to be discontinuous, following discontinuities in path curvature, and hence dynamically

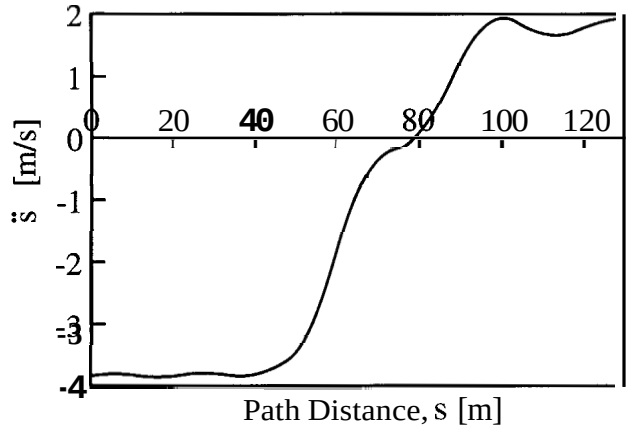

Figure 18: Acceleration limit for lane change maneuver

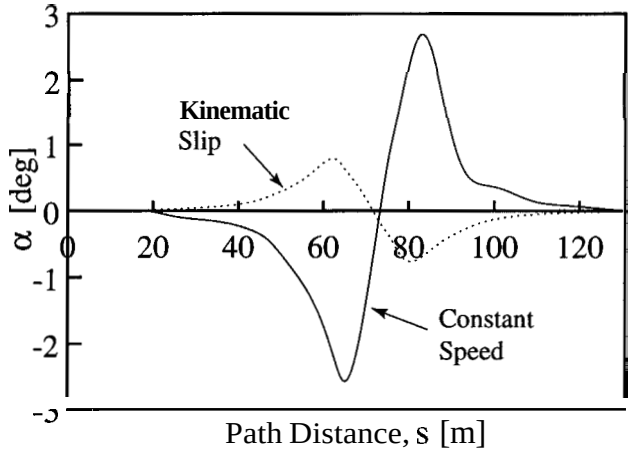

Figure 19: Slip angle for maximum constant speed along the lane change maneuver

infeasible, considering the nonzero dynamics of the steering actuator. The transient steering is also shown to oscillate due to the oscillatory nature of the body slip angle, which depends on the vehicle speed.

The use of the velocity limit curve for generating emergency maneuvers is demonstrated for a lane change at a constant speed. Independently computing the highest constant speed maneuver that does not violate the control constraints resulted in a trajectory that is tangent to the lowest point of the velocity limit curve. Obviously, this maneuver could have been selected without any computation simply by searching over the velocity limit curve. Other potential maneuvers, starting at higher speeds, can be generated by cruising at a constant speed, or accelerating, until hitting the velocity limit curve, then sliding along the velocity limit until completing the lane change.

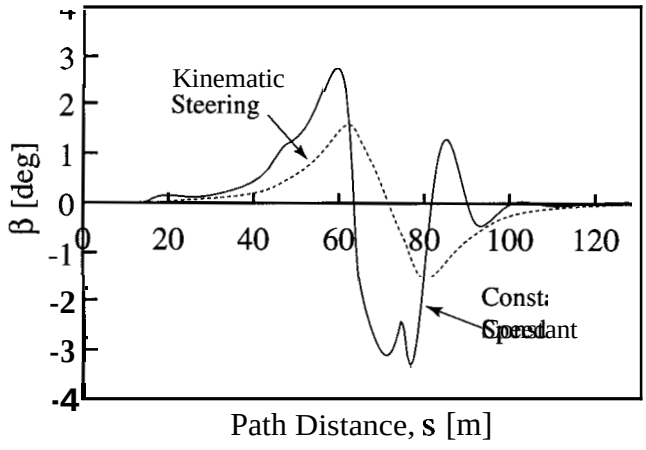

Figure 20: Steering angle for maximum constant speed along the lane change maneuver

Although considering only a simple planar vehicle model, this work provides invaluable insights into the dynamic behavior of ground vehicles, which might not be apparent when using separate lateral and longitudinal models.

This work is summarized in (Shiller and Sundar 1995), and is implemented in a computer program on a Silicon Graphics workstation with interactive graphics. The program computes the nominal steering and tractive force along any path, which can be specified interactively, and the time optimal velocity profile along the path between any boundary speeds.

References

Allen, R.W., H.J., Szostak, T.J., Rosenthal, D.H., Klyde, and K.J., Owens. 1991. "Characteristics influencing ground vehicle lateral/directional dynamic stability," SAE Paper No. 910234.

Chee, W., and M., Tomizuka. 1994. "Lane Change Maneuver of Automobiles for the Intelligent Vehicle and Highway System (IVHS)," American Control Conference, pp. 3586-3587.

Dugoff, H., P.S. Fancher, L. Segel. 1970. "An Analysis of Tire Properties and Their Influence on Vehicle Dynamics Perforamce," SAE Transactions 700377.

Frere, P., 1992. *Sports Cur and Competition Driving,* Robert Bentley Publishing, Cambridge, MA.

Godbole, D. and J. Lygeros, 1994, "Longitudinal Control of the Lead Car of a Platoon", *IEEE Transactions on Vehicular Technology,* Volume 43, Number 4, Pages 1125-1135.

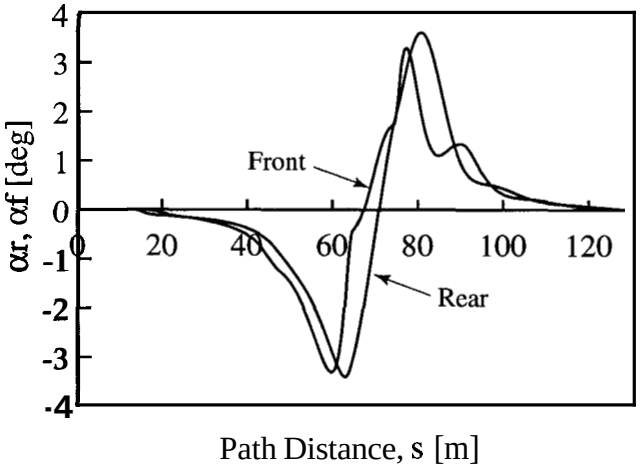

Figure 21: Tire slip angles for maximum constant speed along the lane change maneuver

Hessburg, T., and M., Tomizuka. 1991. "A Fuzzy Rule-Based Controller for Automotive Vehicle Guidance," PATH Research Report, UCB-ITS-PRR-91-18, August.

Hessburg, T., H., Peng, and M., Tomizuka. 1991. "An Experimental Study on Lateral Control of a Vehicle," American Control Conference, pp. 3084-3089.

Lunger, P., "The Influence of the Structure of Automobile Models and Tire Characteristics on the Theoretical Results of Stead-State and Transient Vehicle Performance," The Dynamics of Vehicle, Proceedings 5th VSD-2nd IUTAM Symposium.

Maalej, A.Y., Guenther, D.A., and J.R., Ellis. 1989. "Experimental Development of Tire Force and Moment Models," *International Journal of Vehicle Design*, Vol. 10, No. 1, pp. 34-50.

Narendran, V.K., and J.K., Hedrick. 1993. "Transition Maneuvers in Intelligent Vehicle Highway Systems," Proc. of Conference on Decision and Control, San Antonio, TX, December, pp. 1880-1884.

Peng, H., and M., Tomizuka. 1990. "Lateral Control of Front-Wheel-Steering Rubber-Tire Vehicles," PATH Report, UCB-ITS-PRR-90-5.

Peng, H., and M., Tomizuka. 1991. "Preview Control for Vehicle Lateral Guidance in Highway Automation", American Control Conference, pp. 3090-3095.

Sakai, H., 1981. "Theoretical and Experimental Studies on the Dynamic Properties of Tires," *International Journal of Vehicle Design*, Vol. 2, No. 1.

Sheikholeslam, S., and C.A., Desoer. 1992. "Combined longitudinal and lateral control of a platoon of vehicles," ACC, pp. 1763-1767.

Shiller, Z., and H.H., Lu. 1992. "Computation of Path Constrained Time Optimal Motions along Specified Paths," *ASME J. of Dynamic Systems, Measurement and Control*, Vol. 114, No. 3, pp. 34-40, March.

Shiller, Z., and S., Sundar. 1995. "Emergency Maneuvers for AHS Vehicles," Submitted to SAE Future Transportation Technologies Conference, August.

Smith, D.E., and J.M., Starkey. 1994. "Effects of model complexity on the performance of automated vehicle steering controller: controller development and evaluation," *Journal of Vehicle System Dynamics*, 23, pp. 627-645.